frontiers | Frontiers in Earth Science

TYPE Brief Research Report
PUBLISHED 04 October 2023
DOI 10.3389/feart.2023.1252579

OPEN ACCESS

EDITED BY
Wei-Qiang Ji,
Chinese Academy of Sciences (CAS), China

REVIEWED BY
Tong Liu,
Chinese Academy of Sciences (CAS), China
Sebastian Tappe,
UiT The Arctic University of Norway, Norway

*CORRESPONDENCE
Jing Sun,
sunjingvv@163.com

RECEIVED 04 July 2023
ACCEPTED 18 September 2023
PUBLISHED 04 October 2023

CITATION
Sun J, Jiang L and Sun J (2023), *In situ* U–Pb age determination of apatite from carbonatite and kimberlite in the Batain Basin, eastern Oman.
Front. Earth Sci. 11:1252579.
doi: 10.3389/feart.2023.1252579

In situ U–Pb age determination of apatite from carbonatite and kimberlite in the Batain Basin, eastern Oman

Jing Sun[1,2]*, Leiyin Jiang[2] and Jiaxuan Sun[2]

[1]State Key Laboratory of Petroleum Resources and Engineering, Beijing, China, [2]College of Geosciences, China University of Petroleum, Beijing, China

Northeastern Oman is characterized by carbonatite and kimberlite complexes, which are the ideal samples for studying the relationship between carbonatite and kimberlite. However, the ages of the Oman kimberlite and carbonatite complexes are still unknown, which restricts the understanding of the relationship between carbonatite and kimberlite in Oman. In this study, we use *in situ* laser ablation inductively coupled plasma mass spectrometry (LA-ICPMS) to analyze the apatite from Oman carbonatite, kimberlite, and spessartite. The U–Pb apatite ages are 141.6 ± 6.0 Ma, 137.4 ± 5.2 Ma, and 141.2 ± 6.2 Ma for carbonatite, spessartite (a kind of calc-alkaline lamprophyre), and kimberlite, respectively. These results suggest that the carbonatite and kimberlite were emplaced contemporaneously, followed by calc-alkaline carbonatite (spessartite) emplaced in the Early Cretaceous. The occurrence of carbonatite, kimberlite, and spessartite magmatism of Oman was contemporaneous with the time of the Gondwana breakup during the opening of the Indian Ocean. It is seen that 140 Ma–130 Ma is one of the strongest global kimberlite abundance peaks of the 250 Ma–50 Ma kimberlite bloom, which corresponds with the period of the Pangea supercontinent breakup. The Oman kimberlites and carbonatites are related to a distal effect of the breakup of the Gondwana portion of the Pangea supercontinent, which provided a cool, volatile-fluxed decompression-related circumstance for the formation.

KEYWORDS

U–Pb dating, apatite, Oman, carbonatite, kimberlite, spessartite

1 Introduction

Kimberlite and carbonatite magmatism occurred on continental shields worldwide (Donnelly et al., 2012). Carbonatites are enriched in rare elements, such as niobium and rare earth elements, and may host deposits of these elements. Kimberlite, however, is a unique ultramafic rock derived from the deep mantle and a host of diamonds (Mitchell, 1986; Mitchell, 1995; Woolley et al., 1996). Carbonatites and kimberlites are all volumetrically minor components of continental magmatism, but they are fundamentally significant for our understanding of the carbon cycle, mantle evolution, and deep melting events. Studies have demonstrated that both kimberlite and carbonatite are among the deepest probes in the geochemical cycle (Bizimis et al., 2003; Nowell et al., 2004; Tappe et al., 2007; Ernst and Bell, 2010; Tappe et al., 2017), and it is imminent that recycling volatile-rich components from the Earth's surface into the mantle is required to create the source regions

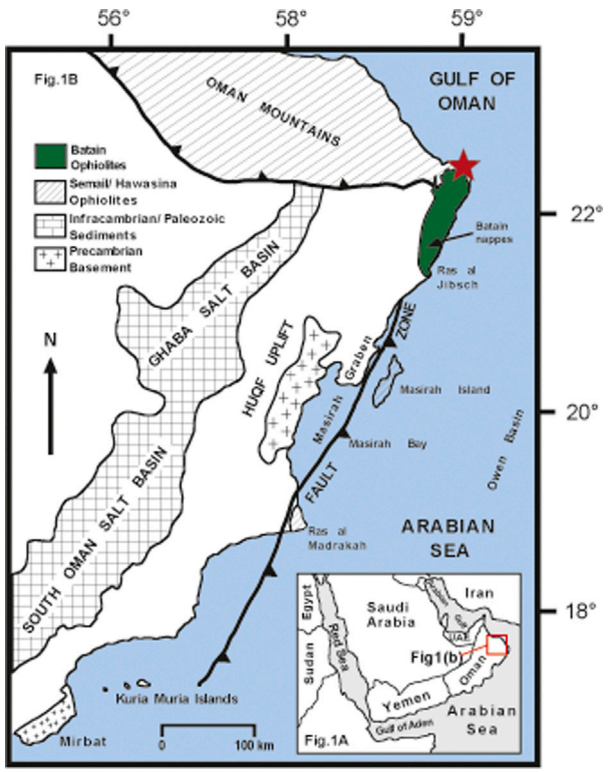

FIGURE 1
Geologic map of the northeastern Oman margin showing the location of carbonatite, spessartite, and kimberlite. Modified from Ries and Shackleton, (1990). The red star represents where the sample is collected.

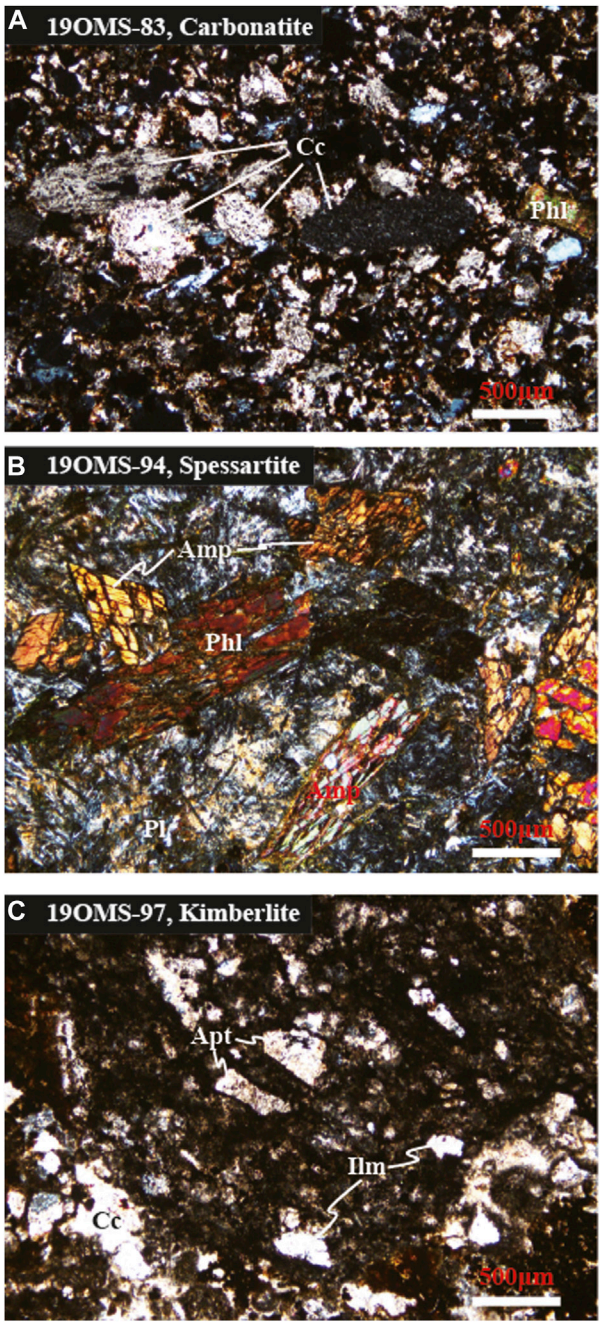

FIGURE 2
Photomicrograph of Oman carbonatite **(A)**, spessartite **(B)**, and kimberlite **(C)** in this study. Amp, amphibole; phl, phlogopite; pl, plagioclase; cc, carbonate; apt, apatite; ilm, ilmenite.

for these two magma types (Bell and Simonetti, 2010; Tappe et al., 2013; Tappe et al., 2017). Kimberlite and carbonatite are commonly observed at the same place on ancient cratons, which raises the questions regarding their temporal distribution and origins. Regarding the view that kimberlite, carbonatite, and lamproite are genetically related, there are strong opinions both in support (Gaspar and Wyllie, 1984; Haggerty, 1989; Haggerty and Fung, 2006; Tappe et al., 2008; Smith et al., 2013; Tappe et al., 2013) and against it (Mitchell, 1979). One school of thought argues that primary carbonatite melts transform into hybrid carbonated silicate magmas akin to kimberlites by assimilation of cratonic mantle material (Tappe et al., 2020), whereas others suggest that kimberlites are not associated with major carbonatite complexes (Smith et al., 2013). The primary task in understanding the relationship between carbonatite and kimberlite is to identify their emplacement times. Additionally, the ages of carbonatite and kimberlite also play a significant role in discovering the linkage between mantle-sourced volatile-rich ultramafic magmas and tectonic processes (Tappe et al., 2020).

Oman is one of the key regions where the carbonatite and kimberlite association occurs and offers a good opportunity to study the kimberlite–carbonatite association. The key to solving these issues is high-precision emplacement ages. However, unlike granulite, carbonatite and kimberlite are all SiO_2-undersaturated rocks containing very rare zircon. Although some studies have reported the U–Pb ages of zircon in carbonatite from Oman, the origin of these zircon grains is still unknown. Although U–Pb studies of baddeleyite, perovskite, and apatite from carbonatites and kimberlites have been reported in other places (e.g., Sun et al., 2014; Sun et al., 2022 and references therein), such accessory minerals have not been found and studied in Oman kimberlite and carbonatite so far. In this study, we use apatite from the Oman carbonatite, spessartite [one type of calc-alkaline lamprophyre based on the classification of Rock (1986); Tappe et al. (2005)], and kimberlite to date their emplacement times, which would be

important in understanding the relationship between kimberlite and carbonatite in Oman in further studies, and the associated tectonic processes would also be discussed.

2 Geological background

Samples in this study were collected from Batain Nappes in the eastern Oman Mountains (Figure 1). The Batain Basin was situated at the junction of Arabia, India, Eurasia/Iran, and northeastern Oman until the opening of the Neotethys in the Early Permian (Figure 1A). The geology of the Batain Basin (part of the early Indian Ocean) in eastern Oman is dominated by the Batain Nappes, which comprise an allochthonous sequence of Permian to uppermost Cretaceous marine sedimentary and volcanic rocks (Nasir et al., 2011). The creation of the Batain Basin was led by the separation of Gondwana in the latest Carboniferous/Early Permian (Schreuer and Immenhauser, 1999; Hauser et al., 2001; Nasir et al., 2011), and it is dominated by the Batain Nappes (Nasir et al., 2011), which show two thrust sheets composed of the latest Jurassic (~150 Ma) ophiolite and a mid-Cretaceous alkali basaltic sequence (115 Ma–125 Ma) (Meyer et al., 1996; Peters and Mercolli, 1998). The Batain Nappes are built by the lower Permian Qarari Formation, the upper Permian Mathbat Formation, the Middle Jurassic to Lowermost Cretaceous Ruwayda Formation, the Oxfordian to Santonian Wahra Formation, and the Santonian to uppermost Maastrichtian Fayah Formation (Gnos et al., 1997). Alkaline volcanic rocks abound within the Wahra and Ruwayda formations, which reflect an active alkaline sea-floor magmatism that produced seamount structures and many dispersed extrusive and intrusive rocks in the Wahra Formation. The UML and carbonatite are found only within the Wahra Formation, with outcrops spanning across the entire Batain Plain.

Samples in this study, including carbonatite, kimberlite, and spessartite, are from Batain Nappes, eastern Oman (Figure 1B). Carbonatite is associated with alkaline rocks and basalt, and their wall rock is composed of Triassic limestone. Spessartite is the dyke cutting through aillikite. Carbonatite (19OMS-83, Figure 2A) is composed of approximately 70% calcite and dolomite. Accessory minerals include ilmenite, phlogopite, barite, and apatite. Spessartite (19OMS-94, Figure 2B) has a porphyroclastic texture with amphibole and minor phlogopite in the phenocryst. The groundmass in this sample has calcite flow texture, which has carbonated plagioclase and minor amphibole, phlogopite, ilmenite, and barite. Based on the classification of Rock (1986) and Tappe et al. (2005), spessartite belongs to the calc-alkaline lamprophyre. Kimberlite (19OMS-97, Figure 2C) contains megacrysts of serpentinized olivine, garnet, diopside, carbonate minerals (Fe-rich dolomite and calcite), chromite, ilmenite, and apatite.

3 Analytical methods

Separated mineral grains of apatite were handpicked, mounted in epoxy resin, and polished until the centers of the grains were exposed. Before isotopic analysis, back-scattered electron (BSE) images were obtained using a JEOL JXA8100 electron microprobe in order to assess internal compositional variation and textures and identify potential target sites for U–Pb analyses.

U–Pb isotopic analyses of apatite from three samples (19OMS-83, 19OMS-94, and 19OMS-97) were performed on an Agilent 7900 ICP-MS instrument (Agilent Technology, Tokyo, Japan) combined with a 193-nm ArF excimer laser (Geolas HD, MicroLas Göttingen, Germany) at the State Key Laboratory of Geological Processes and Mineral Resources, China University of Geosciences, Wuhan. The laser spot size is 44 μm with a fluence of 8 J/cm^2 in this study. Then, the ablated material was transported to ICP using high-purity argon (makeup gas) and helium (carrier gas) (Luo et al., 2018a). To enhance accuracy and precision, a trace amount of water vapor was added before the ablation cell (Luo et al., 2018b; Luo et al., 2020), and a data processing device, serving as a fully interactive mercury signal reductant (Hu et al., 2014) and facilitating signal smoothing and mercury removal, was used in this laser ablation system to obtain ICP data. The counting times were 20 s for background signal acquisition and 50 s after ablation for each single-spot analysis. MAD apatite was used as the external standard to correct the Pb/U fractionation and instrumental mass discrimination. All initial common Pb were corrected using VizualAge in Iolite software. Uncertainties on individual analyses and pooled ages are reported at the 2s level. During the analytical sessions, the Otter Lake apatite has been repeatedly analyzed as unknown, and it yielded a lower intercept age of 916 ± 19 Ma (MSWD=23, n=30), which is consistent with its reference age (913 ± 7, Barfod et al., 2005).

4 U–Pb ages of apatite

The U–Pb isotope data on apatite grains from Oman kimberlite, carbonatite, and spessartite are listed in Table 1 and shown in Figure 3. As shown by LA-ICPMS data, the apatite grains have high U (3.1–47.8 ppm) and Th (16.3–366 ppm) contents that are favorable for U–Pb age determinations. Apatite grains from all three samples show a large Pb isotopic variation and less Pb loss. On the Tera–Wasserburg diagram, data points define a discordia line with a lower intercept age of 141.6 ± 6.0 Ma (MSWD = 0.71, n = 20) for carbonatite, 137.4 ± 5.2 Ma (MSWD = 1.5, n = 20) for spessartite, and 141.2 ± 6.2 Ma (MSWD=1.15, n = 20) for kimberlite. Therefore, these data indicate that three samples of apatite from the Oman carbonatite, spessartite, and kimberlite yield almost the same U-Pb ages of ~140 Ma.

5 Discussion

Previous studies used zircon and phlogopite grains to date carbonatite (Peters et al., 2001), ultramafic lamprophyric sills, and glimmerite xenoliths within the aillikite (Nasir et al., 2008) within the Batain Nappes, northeastern Oman. Ar-Ar ages of phlogopite in ultramafic lamprophyric sills and glimmerite xenoliths within the aillikite are 154 Ma–162 Ma (Nasir et al., 2008) and 150 ± 2 Ma, respectively (Peters et al., 2001). Zircon from carbonatites produced a weighted average $^{206}Pb/^{238}U$ age of 137 ± 1 Ma (Nasir et al., 2011). However, the analyzed mineral,

TABLE 1 U-Pb isotopic compositions of apatites from Oman rocks.

Sample No.	GPS	Rock type	$^{206}Pb/^{238U}$	2SE	$^{207}Pb/^{206}Pb$	2SE	U (ppm)	2SE	Th (ppm)	2SE	Pb (ppm)	2SE	rho $^{207}Pb/^{206}Pb$ v $^{238}U/^{206}Pb$	rho $^{206}Pb/^{238}U$ v $^{207}Pb/^{235}U$
19OMS83-1	22°29'44.34", 59°41'46.35"	Carbonatite	0.1259	0.0025	0.5347	0.0135	16.4	0.2	56.7	2.1	13.4	0.3	0.5411	0.2782
19OMS83-2		Carbonatite	0.1605	0.0025	0.5709	0.0124	15.6	0.2	53.5	0.8	16.7	0.3	0.5584	0.2161
19OMS83-3		Carbonatite	0.2621	0.0039	0.5887	0.0103	20.4	0.4	250.8	2.9	40.4	0.6	0.5530	0.3468
19OMS83-4		Carbonatite	1.2270	0.0524	0.6314	0.0057	13.1	0.7	366.0	5.0	118.4	1.9	0.1010	0.9765
19OMS83-5		Carbonatite	0.1127	0.0025	0.5313	0.0102	40.0	0.4	161.5	5.0	30.1	0.5	0.3768	0.6532
19OMS83-6		Carbonatite	0.1246	0.0019	0.5378	0.0109	28.4	0.5	72.2	1.3	22.1	0.5	0.6338	0.1908
19OMS83-7		Carbonatite	0.2007	0.0046	0.5798	0.0180	8.53	0.2	34.9	0.6	11.3	0.3	0.7160	0.0480
19OMS83-8		Carbonatite	0.1290	0.0032	0.5338	0.0159	13.7	0.4	66.7	1.8	11.5	0.3	0.3901	0.3989
19OMS83-9		Carbonatite	0.0809	0.0015	0.4800	0.0108	43.4	1.0	137.7	3.0	20.5	0.5	0.6762	0.2507
19OMS83-10		Carbonatite	0.1025	0.0015	0.5109	0.0116	35.1	0.7	127.7	2.4	22.5	0.5	0.6322	0.0055
19OMS83-11		Carbonatite	0.0873	0.0013	0.4920	0.0113	36.2	0.8	226.2	5.5	21.6	0.5	0.6888	-0.0326
19OMS83-12		Carbonatite	0.1018	0.0017	0.5129	0.0118	28.7	0.5	88.8	1.7	18.3	0.4	0.4920	0.2407
19OMS83-13		Carbonatite	0.1280	0.0023	0.5391	0.0143	24.1	0.3	71.8	1.3	19.6	0.4	0.6289	0.0748
19OMS83-14		Carbonatite	0.0898	0.0019	0.4982	0.0145	22.5	0.2	73.3	0.7	12.1	0.2	0.4840	0.2879
19OMS83-15		Carbonatite	0.1817	0.0038	0.5648	0.0119	15.6	0.5	87.0	2.8	18.7	0.6	0.5672	0.3992
19OMS83-16		Carbonatite	0.1036	0.0017	0.5162	0.0131	27.3	0.5	74.0	1.5	18.7	0.4	0.7165	-0.0629
19OMS83-17		Carbonatite	0.1224	0.0034	0.5179	0.0145	12.8	0.5	52.5	0.7	11.1	0.2	0.4577	0.5280
19OMS83-18		Carbonatite	0.2706	0.0029	0.5907	0.0080	30.3	0.6	303.4	5.4	66.7	1.2	0.4422	0.3640
19OMS83-19		Carbonatite	0.0862	0.0022	0.4844	0.0111	39.9	2.2	126.5	5.4	22.5	0.8	0.0148	0.7522
19OMS83-20		Carbonatite	0.2340	0.0041	0.5880	0.0131	14.8	0.3	145.6	3.2	28.8	0.6	0.5804	0.2277
19OMS94-01	22°10'14.36",59°38'13.94"	Spessartine	0.0347	0.0016	0.3607	0.0328	14.6	0.7	99.5	5.1	1.8	0.1	0.5643	0.0407
19OMS94-02		Spessartine	0.0379	0.0019	0.3684	0.0277	16.2	0.3	110.9	2.3	2.2	0.1	0.3322	0.3430
19OMS94-03		Spessartine	0.0381	0.0018	0.4007	0.0315	13.5	0.4	86.7	2.2	1.8	0.1	0.5713	0.1287
19OMS94-04		Spessartine	0.0341	0.0014	0.3209	0.0218	22.0	0.4	141.3	1.6	2.5	0.1	-0.0497	0.6631
19OMS94-05		Spessartine	0.0315	0.0015	0.2730	0.0225	20.9	0.8	135.1	6.5	2.3	0.1	0.4291	0.2317
19OMS94-06		Spessartine	0.0427	0.0024	0.4643	0.0393	13.6	1.1	96.7	8.6	2.1	0.2	0.2727	0.4630
19OMS94-07		Spessartine	0.0450	0.0039	0.4425	0.0629	20.6	1.9	140.2	13.2	3.4	0.1	-0.2568	0.5623
19OMS94-08		Spessartine	0.0375	0.0022	0.3742	0.0333	12.8	0.7	89.9	6.2	1.7	0.1	0.3938	0.3632
19OMS94-09		Spessartine	0.0474	0.0053	0.4733	0.0880	22.2	0.5	153.8	2.6	3.8	0.4	-0.0689	0.5210
19OMS94-10		Spessartine	0.1157	0.0143	0.6444	0.0375	11.6	0.3	64.3	1.7	4.2	0.5	-0.2379	0.9490
19OMS94-11		Spessartine	0.0684	0.0086	0.4936	0.0409	17.8	0.7	112.2	5.3	3.8	0.4	-0.6286	0.9367
19OMS94-12		Spessartine	0.0315	0.0011	0.2664	0.0178	27.3	0.7	183.1	3.8	3.1	0.1	0.1808	0.2997
19OMS94-13		Spessartine	0.0340	0.0014	0.3228	0.0214	18.3	0.9	123.9	5.3	2.1	0.1	0.3962	0.2854
19OMS94-14		Spessartine	0.0339	0.0016	0.3256	0.0272	17.3	0.5	107.6	5.1	2.0	0.1	0.2389	0.2461
19OMS94-15		Spessartine	0.0312	0.0013	0.2946	0.0238	22.8	0.7	151.3	4.9	2.4	0.1	0.5590	-0.1484
19OMS94-16		Spessartine	0.0428	0.0040	0.3866	0.0410	17.8	1.8	119.5	12.7	2.3	0.2	-0.3766	0.8181
19OMS94-17		Spessartine	0.0480	0.0028	0.4337	0.0256	19.0	1.4	130.0	10.7	3.1	0.2	-0.0075	0.7189

(Continued on following page)

TABLE 1 (*Continued*) U-Pb isotopic compositions of apatites from Oman rocks.

Sample No.	GPS	Rock type	$^{206}Pb/^{238U}$	2SE	$^{207}Pb/^{206}Pb$	2SE	U (ppm)	2SE	Th (ppm)	2SE	Pb (ppm)	2SE	rho $^{207}Pb/^{206}Pb$ v $^{238}U/^{206}Pb$	rho $^{206}Pb/^{238}U$ v $^{207}Pb/^{235}U$
19OMS94-18		Spessartine	0.0341	0.0022	0.2986	0.0327	19.9	0.4	131.0	2.1	2.4	0.1	0.3018	0.3571
19OMS94-19		Spessartine	0.0309	0.0012	0.2504	0.0157	27.3	0.3	179.3	1.9	2.8	0.1	0.5313	0.1185
19OMS94-20		Spessartine	0.0430	0.0034	0.3977	0.0380	14.7	1.1	94.4	7.3	2.0	0.2	-0.1359	0.7582
19OMS97-1	22°8'57.56",59°37'48.29"	Kimberlite	0.0424	0.0027	0.3444	0.0380	4.61	0.1	43.0	1.3	1.25	0.1	0.5867	0.1443
19OMS97-2		Kimberlite	0.0648	0.0025	0.4302	0.0235	10.7	0.4	16.3	0.4	3.03	0.1	0.6054	0.1823
19OMS97-3		Kimberlite	0.0429	0.0028	0.3390	0.0416	4.54	0.2	41.4	1.6	1.23	0.1	0.5136	-0.0081
19OMS97-4		Kimberlite	0.0552	0.0010	0.3822	0.0098	47.8	0.9	239.3	4.6	14.3	0.3	0.6845	0.0935
19OMS97-5		Kimberlite	0.0414	0.0028	0.3285	0.0333	4.64	0.1	43.1	0.9	1.31	0.1	0.6017	0.0678
19OMS97-6		Kimberlite	0.0863	0.0019	0.4678	0.0148	15.2	0.3	41.6	2.0	8.05	0.2	0.5956	0.0685
19OMS97-7		Kimberlite	0.4154	0.0393	0.5913	0.0213	3.80	0.3	106.0	10.4	11.6	0.3	0.0541	0.9154
19OMS97-8		Kimberlite	0.0453	0.0027	0.3258	0.0300	3.78	0.1	42.6	0.4	1.14	0.1	0.6512	0.0843
19OMS97-9		Kimberlite	0.0483	0.0034	0.3603	0.0370	3.65	0.1	39.2	0.5	1.13	0.1	0.3637	0.4123
19OMS97-10		Kimberlite	0.0408	0.0027	0.3188	0.0408	4.54	0.1	47.6	1.6	1.15	0.1	0.3246	-0.1179
19OMS97-11		Kimberlite	0.0572	0.0014	0.4149	0.0167	22.7	0.6	61.5	5.4	7.59	0.2	0.5914	0.0153
19OMS97-12		Kimberlite	0.0405	0.0028	0.2771	0.0351	4.48	0.2	44.7	1.2	1.16	0.1	0.7688	0.0307
19OMS97-13		Kimberlite	0.0390	0.0024	0.2711	0.0271	4.51	0.1	48.7	0.5	1.28	0.1	0.7087	-0.0512
19OMS97-14		Kimberlite	0.0676	0.0021	0.4236	0.0192	9.72	0.2	22.8	0.4	3.16	0.1	0.6419	-0.0230
19OMS97-15		Kimberlite	0.0388	0.0026	0.2850	0.0312	5.11	0.1	53.7	0.6	1.31	0.1	0.5461	0.0548
19OMS97-16		Kimberlite	0.0395	0.0022	0.2987	0.0305	5.13	0.1	54.3	0.6	1.12	0.1	0.5808	-0.0279
19OMS97-17		Kimberlite	0.0415	0.0025	0.3439	0.0360	3.83	0.1	41.2	1.1	0.92	0.1	0.4180	0.0863
19OMS97-18		Kimberlite	0.0849	0.0063	0.4458	0.0191	24.0	3.3	105.6	9.3	9.78	0.2	-0.6462	0.9318
19OMS97-19		Kimberlite	0.1719	0.0044	0.5393	0.0170	8.81	0.2	49.3	0.7	9.72	0.2	0.4769	0.3060
19OMS97-20		Kimberlite	0.0541	0.0043	0.3706	0.0465	3.06	0.2	31.2	1.8	0.75	0.1	0.4751	0.3121

phlogopite, is not a suitable mineral for Ar-Ar geochronology due to the existence of excess Ar. As for the zircons, studies suggested that some zircons in mantle-sourced rocks, such as kimberlite, may be of crustal origin extracted by host magma, which would yield a crustal age rather than an emplaced age (Sun, 2022). Moreover, the age of the kimberlite from Oman has not been studied so far.

Apatite crystallizes directly from the magmas and contains enough U for precise Pb isotopic analyses, which provides an excellent opportunity to remove the uncertainties in the determination of the age of the Oman kimberlite and carbonatite, thus making the U–Pb age determination reliable (Wu et al., 2013). The apatite U–Pb ages indicate that carbonatite and kimberlite were contemporaneous with a weighted average of 141 Ma, which is relatively earlier than the calc-alkaline lamprophyre (spessartite; 137 Ma). We consider the ages in this study to be the best estimate of the emplacement time of kimberlite, carbonatite, and calc-alkaline lamprophyre in Batain Nappes from Oman. Hence, the kimberlite and carbonatite from Oman emplaced at 141 Ma, followed by calc-alkaline carbonatite (spessartite) emplaced at 137 Ma, suggesting a complex magmatic plumbing system existed beneath the Batain Basin of the Oman field. The results of this study are significant in understanding the relationship between kimberlite and carbonatite associations in Oman, which can extend to a global scale in further studies.

The global kimberlite record suggests that approximately 80% of known occurrences are linked to breakup stages of supercontinents, and the others are collision-induced (Jelsma et al., 2009; Tappe et al., 2018; Zhang et al., 2019). The Indian Ocean was a stepwise breakup of east and west Gondwana at 157 Ma, and a breakup of east Gondwana at 130 Ma (Gnos and Perrin, 1996), which is registered only in the Batain Basin of Oman (Hauser et al., 2001). Paleomagnetic data from a previous study also showed that the eastern Oman oceanic lithosphere was formed at latitudes 38° ± 12°S around 150 Ma during the active breakup of Gondwana (Gnos and Perrin, 1996). So it appears that the emplacement of the Early Cretaceous kimberlite and carbonatite magmatism (~140 Ma) in Oman is related to the breakup of Gondwana, and kimberlite and carbonatite occurred during the

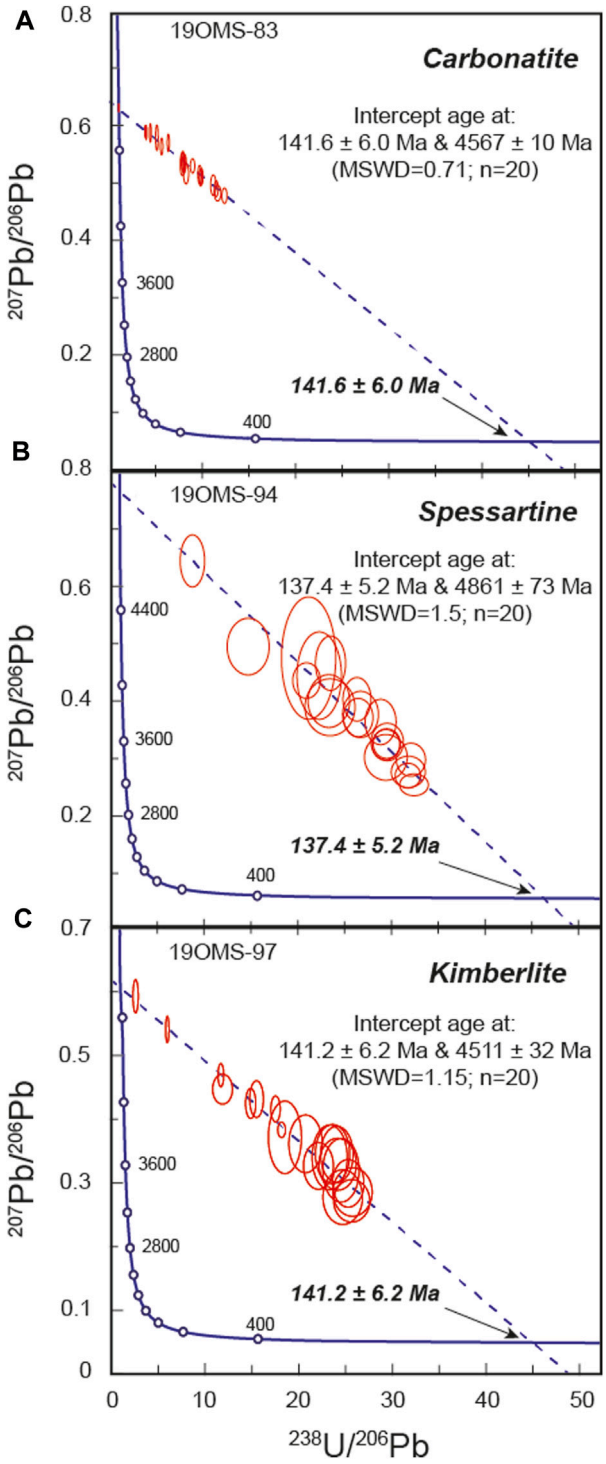

FIGURE 3
U–Pb concordia diagrams after Tera–Wasserburg concordia of the Oman apatite. **(A)** Carbonatite; **(B)** Spessartine; **(C)** Kimberlite.

opening of the Indian Ocean (Peters and Mercolli, 1998). The most critical petrological variables enabling the formation of kimberlite and CO_2-rich ultramafic magmatism are the availability of oxidized CHO volatile species such as CO_2 and H_2O (Yaxley et al., 2017), as well as the lower temperatures of Earth's upper mantle (Green and Falloon, 1998; Tappe et al., 2018). Thus, the breaking up of Gondwana, which releases pressure, provided a relatively cool and volatile-fluxed circumstance for the formation of Oman kimberlite and carbonatite melts.

Mesozoic–Cenozoic kimberlite between 250 Ma and 50 Ma is the most remarkable kimberlite bloom globally, and more than 60% of the world's known kimberlite clusters on every continent were emplaced during this bloom. It was observed that 140 Ma–130 Ma is one of the strongest global kimberlite abundance peaks of this bloom (Figure 8 in Tappe et al., 2018), which corresponds to the period of the Pangea supercontinent breakup (Jelsma et al., 2009). By that time, the Indian Ocean had opened widely and the Gondwana portion of Pangea was separated into West and East Gondwanaland. The Early Cretaceous (~140 Ma) Oman kimberlite, carbonatite, and spessartite were just formed under the tectonic background of the Pangea breakup.

6 Conclusion

Apatite U–Pb age dating implies that the Oman carbonatite, kimberlite, and spessartite are broadly coeval in the Early Cretaceous (137 Ma–140 Ma). The occurrence of carbonatite, kimberlite, and spessartite magmatism in Oman was contemporaneous with the time of the Gondwana breakup during the opening of the Indian Ocean. It was observed that 140 Ma–130 Ma is one of the strongest global kimberlite abundance peaks of the 250 Ma–50 Ma kimberlite bloom, which corresponds to the period of the Pangea supercontinent breakup. The breaking up of the Gondwana portion of the Pangea supercontinent provided a cool, volatile-fluxed decompression-related circumstance for the formation of Oman kimberlite and carbonatite melts.

Data availability statement

The original contributions presented in the study are included in the article/Supplementary Material; further inquiries can be directed to the corresponding author.

Author contributions

JinS wrote the manuscript and designed the idea. LJ conducted U–Pb dating measurement and processed the data. JiaS performed U–Pb dating measurement. All authors contributed to the article and approved the submitted version.

Conflict of interest

The authors declare that the research was conducted in the absence of any commercial or financial relationships that could be construed as a potential conflict of interest.

Publisher's note

All claims expressed in this article are solely those of the authors and do not necessarily represent those of their affiliated

organizations, or those of the publisher, the editors, and the reviewers. Any product that may be evaluated in this article, or claim that may be made by its manufacturer, is not guaranteed or endorsed by the publisher.

References

Barfod, G. H., Krogstad, E. J., Frei, R., and Albarède, F. (2005). Lu-Hf and PbSL geochronology of apatites from proterozoic terranes: A first look at Lu-Hf isotopic closure in metamorphic apatite. *Geochim. Cosmochim. Acta* 69, 1847–1859. doi:10.1016/j.gca.2004.09.014

Bell, K., and Simonetti, A. (2010). Source of parental melts to carbonatites — Critical isotopic constraints. *Min. Petrol.* 98, 77–89. doi:10.1007/s00710-009-0059-0

Bizimis, M., Salters, V. J. M., and Dawson, J. B. (2003). The brevity of carbonatite sources in the mantle: evidence from Hf isotopes. *Contrib. Mineral. Petrol.* 145, 281–300. doi:10.1007/s00410-003-0452-3

Donnelly, C. L., Griffin, W. L., Yang, J. H., O'Reilly, S. Y., Li, Q. L., Pearson, N. J., et al. (2012). *In situ* U-Pb dating and Sr-Nd isotopic analysis of perovskite: constraints on the age and petrogenesis of the kuruman kimberlite province, kaapvaal craton, South Africa. *J. Petrol.* 53, 2497–2522. doi:10.1093/petrology/egs057

Ernst, R. E., and Bell, K. (2010). Large igneous provinces (LIPs) and carbonatites. *Min. Petrol.* 98, 55–76. doi:10.1007/s00710-009-0074-1

Gaspar, J. C., and Wyllie, P. J. (1984). The alleged kimberlite-carbonatite relationship: evidence from ilmenite and spinel from premier and wesselton mines and the benfontein sill, South Africa. *Contrib. Mineral. Petrol.* 85 (2), 133–140. doi:10.1007/bf00371703

Gnos, E., Immenhauser, A., and Peters, T. (1997). Late Cretaceous early Tertiary convergence between the Indian and Arabian Plates recorded in ophiolites and related sediments. *Tectonophysics* 271, 1–19. doi:10.1016/s0040-1951(96)00249-1

Gnos, E., and Perrin, M. (1996). Formation and evolution of the Masirah ophiolite constrained by paleomagnetic study of volcanic rocks. *Tectonophysics* 253, 53–64. doi:10.1016/0040-1951(95)00056-9

Green, D. H., and Falloon, T. J. (1998). "Pyrolite: A ringwood concept and its current ex-pression," in *The Earth's mantle*. Editor I. Jackson (Cambridge: Cambridge University Press), 311–378.

Haggerty, S. E., and Fung, F. (2006). Orbicular oxides in carbonatitic kimberlites. *Am. Mineral.* 91, 1461–1472. doi:10.2138/am.2006.2194

Haggerty, S. E. (1989). "Mantle metasomes and the kinship between carbonatites and kimberlites," in *Carbonatites: Genesis and evolution*. Editor K. Bell (London: Academic Division, Unwin Hyman Ltd.), 546–560.

Hauser, M., Martini, R., Burns, S., Dumitrica, P., Kristyn, L., Matter, A., et al. (2001). Triassic stratigraphic evolution of the Arabian-Greater India embayment of the southern Tethys margin. *Ecol. Geol. Helv.* 94, 29–62. doi:10.1144/GSL.SP.2001.185.01.15

Hu, Z. C., Zhang, W., Liu, Y. S., Gao, S., Li, M., Zong, K. Q., et al. (2014). "Wave" signal-smoothing and mercury-removing device for laser ablation quadrupole and multiple collector ICPMS analysis: application to lead isotope analysis. *Anal. Chem.* 87, 1152–1157. doi:10.1021/ac503749k

Jelsma, H., Barnett, W., Richards, S., and Lister, G. (2009). Tectonic setting of kimberlites. *Lithos* 112, 155–165. doi:10.1016/j.lithos.2009.06.030

Luo, T., Hu, Z. C., Zhang, W., Günther, D., Liu, Y. S., Zong, K. Q., et al. (2018a). Reassessment of the influence of carrier gases He and Ar on signal intensities in 193 nm excimer LA-ICP-MS analysis. *J. Anal. At. Spectrom.* 33, 1655–1663. doi:10.1039/c8ja00163d

Luo, T., Hu, Z. C., Zhang, W., Liu, Y. S., Zong, K. Q., Zhou, L., et al. (2018b). Water vapor-assisted "universal" nonmatrix-matched analytical method for the *in situ* U-Pb dating of zircon, monazite, titanite, and xenotime by laser ablation-inductively coupled plasma mass spectrometry. *Anal. Chem.* 90, 9016–9024. doi:10.1021/acs.analchem.8b01231

Luo, T., Zhao, H., Li, Q. L., Li, Y., Zhang, W., Guo, J. L., et al. (2020). Non-matrix-matched determination of Th-Pb ages in zircon, monazite and xenotime by laser ablation-inductively coupled plasma-mass spectrometry. *Geostand. Geoanalytical Res.* 44, 653–668. doi:10.1111/ggr.12356

Meyer, J., Mercoulli, I., and Immenhauser, A. (1996). Off ridge alkaline magmatism and seamount volcanoes in the Masirah Island ophiolite, Oman. *Tectonophysics* 267, 187–208. doi:10.1016/s0040-1951(96)00094-7

Mitchell, R. H. (1995). *Kimberlites, orangeites, and related rocks*. New York: Plenum Press, 410.

Mitchell, R. H. (1986). *Kimberlites: Mineralogy, geochemistry, and Petrology*. New York: Plenum Press, 442.

Mitchell, R. H. (1979). The alleged kimberlite-carbonatite relationship: additional contrary mineralogical evidence. *Am. J. Sci.* 279, 570–589. doi:10.2475/ajs.279.5.570

Murphy, D. T., Collerson, K. D., and Kamber, B. S. (2002). Lamproites from gaussberg, Antarctica: possible transition zone melts of archaean subducted sediments. *J. Petrol.* 43, 981–1001. doi:10.1093/petrology/43.6.981

Nasir, S., Al-Khirbash, S., Rollinson, H., Al-Harthy, A., Al-Sayigh, A., Al-Lazki, A., et al. (2008). "Late Jurassic to Tertiary kimberlite, carbonatite and lamproite dike swarms from the Bomethra area, Northeastern Oman," in *9th kimberlite conference extended abstract nr 91KC-A-00003*.

Nasir, S., Al-Khirbash, S., Rollinson, H., Al-Harthy, A., Al-Sayigh, A., Al-Lazki, A., et al. (2011). Petrogenesis of early cretaceous carbonatite and ultramafic lamprophyres in a diatreme in the Batain Nappes, Eastern Oman continental margin. *Contrib. Mineral. Petrol.* 161, 47–74. doi:10.1007/s00410-010-0521-3

Nowell, G. M., Pearson, D. G., Bell, D. T., Carlson, R. W., Smith, C., Kempton, P. D., et al. (2004). Hf isotope systematics of kimberlites and their megacrysts: new constraints on their source regions. *J. Petrol.* 45, 1583–1612. doi:10.1093/petrology/egh024

Peters, T., Batttashy, M., Blaesi, H., Hauser, M., Immenhauser, A., Monser, L., et al. (2001). *Geological map of Sur and Al Ashkarah explanatory notes*. Oman Ministry of Commerce and Industry Directorate General Minerals, 95.

Peters, T., and Mercolli, I. (1998). Extremely thin oceanic crust in the proto- Indian ocean: evidence from the masirah ophiolite, sultanate of Oman. *J. Geophys. Res. Solid Earth.* 103, 677–689. doi:10.1029/97jb02674

Prelevic, D., Stracke, A., Foley, S. F., Romer, R. L., and Conticelli, S. (2010). Hf isotope compositions of mediterranean lamproites: mixing of melts from asthenosphere and crustally contaminated mantle lithosphere. *Lithos* 119, 297–312. doi:10.1016/j.lithos.2010.07.007

Rapp, R. P., Irifune, T., Shimizu, N., Nishiyama, N., Norman, M. D., and Inoue, J. (2008). Subduction recycling of continental sediments and the origin of geochemically enriched reservoirs in the deep mantle. *Earth Planet. Sc. Lett.* 271, 14–23. doi:10.1016/j.epsl.2008.02.028

Ries, A. C., and Shackleton, R. M. (1990). "Structures of the huqf–haushi uplift, east-central Oman," in *The geology and tectonics of the Oman region*. Editors A. H. F. Robertson, M. P. Searle, and A. C. Ries (Geological Society of London Special Publication), 49, 715–726.

Rock, N. M. S. (1986). The nature and origin of ultramafic lamprophyres: aln ites and allied rocks. *J. Petrol.* 27, 155–196. doi:10.1093/petrology/27.1.155

Schreuer, G., and Immenhauser, A. (1999). West-northwest-directed obduction of the Batain Group on eastern Oman continental margin at the Cretaceous-Tertiary boundary. *Tectonophysics* 18, 148–160.

Smith, C. B., Haggerty, S. E., Chatterjee, B., Beard, A., and Townend, R. (2013). Kimberlite, lamproite, ultramafic lamprophyre, and carbonatite relationships on the Dharwar craton, India; an example from the Khaderpet pipe, a diamondiferous ultramafic with associated carbonatite intrusion. *Lithos* 182 (12), 102–113. doi:10.1016/j.lithos.2013.10.006

Sun, J., Liu, C. Z., Tappe, S., Kostrovitsky, S. I., Wu, F. Y., Yakovlev, D., et al. (2014). Repeated kimberlite magmatism beneath yakutia and its relationship to siberian flood volcanism: insights from *in situ* U–Pb and Sr–Nd perovskite isotope analysis. *Earth Planet. Sci. Lett.* 404, 283–295. doi:10.1016/j.epsl.2014.07.039

Sun, J. (2022). Trace elements and Hf isotopic compositions of four ancient zircon megacrysts from yakutian kimberlite, siberia: implications for identifying mantle and old zircon megacrysts from kimberlites. *Acta Petrol. Sin.* 37, 3548–3558. (Chinese in English abstract). doi:10.18654/1000-0569/2021.11.18

Tappe, S., Foley, S. F., Jenner, G. A., and Kjasgaard, B. A. (2005). Integrating ultramafic lamprophyres into the IUGS classification of igneous rocks: rationale and implications. *J. Petrol.* 46 (9), 1893–1900. doi:10.1093/petrology/egi039

Tappe, S., Foley, S. F., Kjarsgaard, B. A., Romer, R. F., Heaman, L. M., Stracke, A., et al. (2008). Between carbonatite and lamproite - diamondiferous Torngat ultramafic lamprophyres formed by carbonate-fluxed melting of cratonic MARID-typemetasomes. *Geochim. Cosmochim. AC* 72, 3258–3286. doi:10.1016/j.gca.2008.03.008

Tappe, S., Foley, S. F., Stracke, A., Romer, R. I., Bruce, A., Kjarsgaard, A., et al. (2007). Craton reactivation on the labrador sea margins: $^{40}Ar/^{39}Ar$ age and Sr–Nd–Hf–Pb isotope constraints from alkaline and carbonatite intrusives. *Earth Planet. Sci. Lett.* 256, 433–454. doi:10.1016/j.epsl.2007.01.036

Tappe, S., Pearson, D. G., Kjarsgaard, B. A., Nowell, G. M., and Dowall, D. (2013). Mantle transition zone input to kimberlite magmatism near a subduction zone: origin of anomalous Nd–Hf isotope systematics at lac de Gras, Canada. *Earth Planet. Sci. Lett.* 371, 235–251. doi:10.1016/j.epsl.2013.03.039

Tappe, S., Pearson, D. G., Nowell, G. M., Nielsen, T. F. D., Milstead, P., and Muehlenbachs, K. (2011). A fresh isotopic look at Greenland kimberlites: cratonic

mantle lithosphere imprint on deep source signal. *Earth Planet. Sci. Lett.* 305, 235–248. doi:10.1016/j.epsl.2011.03.005

Tappe, S., Romer, R. L., Stracke, A., Steenfelt, A., Smart, K. A., Muehlenbachs, K., et al. (2017). Sources and mobility of carbonate melts beneath cratons, with implications for deep carbon cycling, metasomatism and rift initiation. *Earth Planet. Sci. Lett.* 466, 152–167. doi:10.1016/j.epsl.2017.03.011

Tappe, S., Smart, K. A., Torsvik, T. H., Massuyeau, M., and de Wit, M. C. J. (2018). Geodynamics of kimberlites on a cooling earth: clues to plate tectonic evolution and deep volatile cycles. *Earth Planet. Sci. Lett.* 484, 1–14. doi:10.1016/j.epsl.2017.12.013

Tappe, S., Stracke, A., Acken, D. V., Strauss, H., and Luguet, A. (2020). Origins of kimberlites and carbonatites during continental collision - insights beyond decoupled Nd-Hf isotopes. *EARTH-SCI Rev.* 208, 103287. doi:10.1016/j.earscirev.2020.103287

Woolley, A. R., Bergman, S., Edgar, A. D., Le Bas, M. J., Mitchell, R. H., Rock, N. M. S., et al. (1996). Classification of the lamprophyres, lamproites, kimberlites, and the kalsilite-, melilite-, and leucite-bearing rocks. *Can. Mineral.* 34, 175–186.

Wu, F. Y., Mitchell, R. H., Li, Q. L., Sun, J., Liu, C. Z., and Yang, Y. H. (2013). *In situ* U-Pb age determination and Sr-Nd isotopic analysis of perovskite from the Premier (Cullinan) kimberlite, South Africa. *Chem. Geol.* 353, 83–95. doi:10.1016/j.chemgeo.2012.06.002

Yaxley, G. M., Berry, A. J., Rosenthal, A., Woodland, A. B., and Paterson, D. (2017). Redox pre-conditioning deep cratonic lithosphere for kimberlite genesis: evidence from the central slave craton. *Sci. Rep.* 7, 30–10. doi:10.1038/s41598-017-00049-3

Zhang, W. B., Johnston, S. T., and Currie, C. A. (2019). Kimberlite magmatism induced by west dipping subduction of the North American plate. *Geology* 47, 395–398. doi:10.1130/G45813.1